Learning-based Restoration Sequence Ordering for Multi-site Traffic Signal Failure

Tingting Zhao[1], Yu Zhang[2,*]

[1] *School of Traffic and Transportation, Beijing Jiaotong University, Beijing 100044, China*
Email: ttzhao@bjtu.edu.cn
[2] *Department of Civil and Environmental Engineering, University of South Florida, 4202 E. Fowler Ave. ENB118, Tampa, FL, 33620, USA*
** Corresponding author: yuzhang@usf.edu*

Abstract

Traffic signal failures could result in significant local and system-level performance degradation. Sequencing the restoration of failed signals with limited resources is a challenging problem—capturing dynamic changing transportation system performance following a feasible solution requires tedious computation, and the short time frame for restoring failed signals makes these decisions time-sensitive and should be determined in a timely manner. Feasible Signal Restoration Sequence Ordering (SRSO) problem, as a critical building block to optimize the restoration sequence, has not been well-studied in the existing literature, nor have solutions to address the computational burden issue. In this work, a machine learning model based on Structural Recurrent Neural Network (SRNN) is proposed to predict system performance, i.e., aggregated accumulated total delay, following a given restoration sequence, to address the computational burden of the simulation-based performance evaluation. Spatio-temporal (ST) graph representation is leveraged in this methodology to take the topological information, i.e., how adjacent movements interact with each other, into consideration. Although microscopic simulation is used to obtain the ground truth performance, which is still time-consuming for a group of signal failure scenarios, a trained machine learning model can surrogate the tedious computation in the decision-making process in a timely manner. The challenges to build this machine learning model effectively and efficiently are two-folds. First, a transportation system is a typical dynamic system whose behavior is constrained by the topology of the network. Therefore, both spatial and temporal interactions between road sections should be captured to predict system performance effectively. Second, in the context of signal failure, system performance is exposed to a disrupted control strategy, which makes it even more challenging to predict system performance effectively. The original SRNN model could address the first challenge, and the movement feature representation and its integration to the SRNN model proposed in this work could address the second. A case study was conducted to demonstrate the operability and effectiveness of the proposed methodology. It is demonstrated that the signal restoration sequence could impact system performance during and after the restoration process significantly. Then, both Aggregated Accumulated Total Delay (AATD) prediction accuracy and the performance of restoration sequence ordering is evaluated for the case study network. Outcomes of the case study show that the learning-based model can help identify sequences ranked in top 8% of optional sequences referring to ground truth information. Furthermore, in terms of the fine-tune of the learning rate, the Cosine-Annealing-LR strategy leads to both lower loss value, better ordering performance, and shorter delay experienced in the restoration process, compared to the Step-LR strategy.

Keywords: Traffic management systems; Emergency response; Machine learning; Learning-based optimization; Ordinal Optimization

1 Introduction

Transportation management systems are typical cyber-physical systems, with sensing, communicating, and computing components integrated to support the efficient operation of transportation systems. These systems are termed as Transportation Cyber-Physical Systems (T-CPS) in this study for convenience. The smooth operation of T-CPS relies on electric power supply and the functionality of sensing and computing components, as premise (Emtenan and Day, 2020). The failure of these supporting components could lead to the failure of a T-CPS system and even cascading failure phenomena in a transportation system. In addition, with the increasing presence of extreme weather conditions (Sadler et al., 2018) such as flooding, thunderstorms, and extreme hot temperature, especially in coastal areas, and emerging cyber security concerns (Ernst and Michaels, 2017; Ghena et al., 2014), there is an increasing number of power outages (Wang et al., 2018), sensing and computational component failures, leading to even more frequent traffic signal failures in real cases, which emphasizes the urgent need to enhance T-CPS system resilience (Mohebbi et al., 2020).

It is well-recognized that the failure of traffic signals, as a critical type and widely existing component of a T-CPS system, could lead to significant transportation system performance degradation and, consequently, significant economy and social functionality loss for society overall. For example, a computer crash disrupted 750 traffic lights in Montgomery County, Maryland, in 2009 and locked traffic in the entire region, which, in turn, increased travel time and the greenhouse gas (GHG) emissions of thousands of vehicles (Halsey, 2009). At a smaller scale, another example is the malfunction of traffic lights at a single intersection in Wellington City, New Zealand, in 2015, that caused severe traffic congestion throughout the main corridor. Even single intersection failures should be taken seriously, as they can create severe traffic congestion if the affected intersections are critical to network performance (Wright and Roberg, 1998) and can cause traffic safety concerns. A signal failure may not cause cascading failure through the transportation management system itself, but its impact on traffic flow propagates through the transportation network. Therefore, the failure of critical signals may lead to congestion in a larger area, i.e., cascading failure in the transportation system. These impacts can be exaggerated if the affected area has severe congestion in its normal condition. These facts highlight the importance of enhancing the resilience of the transportation system against traffic signal failure to support community resilience eventually through countermeasures in the mitigation, preparedness, response, and recovery phases (NGA, 1979).

This study focuses on the failure of multiple traffic signals that occur simultaneously or consecutively in a very short time frame caused by multi-site hazards or cascading failure of the supporting power supply system, sensors, or communication systems. There could be various causes for traffic signal failure; however, the focus of this work is not to investigate the cause of signal failures but rather the post-event phase to evaluate the consequences of traffic signal failures on mobility service and the operational strategy to recover system performance efficiently. As noted, the resources to restore a failed signal could be limited to a great extent, such as a shortage of technical personnel with desired expertise, shortages of equipment or device to repair the failed component, etc. Therefore, although multiple signals must be fixed as quickly as possible, transportation managers must prioritize the restoration effort in reality. Meanwhile, the restoration sequence can impact system performance during and after the restoration process significantly. This statement is consistent with both specialists' understanding and their real-field experience, according to an interview with local transportation management agency. It is also verified in the

case study in Section 4 and further illustrated through the Macroscopic Fundamental Diagram point of view in the appendix of this paper.

In this work, we study the consequences of signal failures at multiple intersections in the post-event phase and propose restoration strategies to recover system performance efficiently given limited labor resources. The objective is to rank optional restoration sequences of multiple failed signals to reduce the impact on system performance, called the Signal Restoration Sequence Ordering (SRSO) problem. To rank the optional restoration sequences of failed traffic signals, system performance under various restoration sequences should be evaluated in a timely manner to support a prompt response to the failure and minimize the potential impact on the system's level of service. In the literature, Accumulated Total Delay has been widely used to evaluate the impact of signal failure on system performance (Ganin et al., 2019). SRSO problem is a critical building block to optimize the signal restoration sequence eventually, especially for heuristic algorithms. Taking Genetic Algorithm (GA) as an example, the ranking, i.e., ordering, of optional restoration sequences is a critical repetitive process embedded in the workflow of the overall solution algorithm.

Compared with the restoration of road infrastructure from a severe nature disaster such as an earthquake, landslide, etc., the time frame to repair failed signals is much shorter. Therefore, it is necessary to capture the dynamic behavior of the system after the signal failure and during the overall restoration process. Either Dynamic Traffic Assignment (Zou and Chen, 2019), mesoscopic (Reilly et al., 2016) or microscopic traffic simulation (Oricchio et al., 2008) could be adopted to conduct a system performance evaluation to address the need to capture the system's dynamic behavior. In this work, the network performance measure, i.e., Aggregated Accumulated Total Delay (AATD), is evaluated through running a microscopic traffic simulation in VISSIM. However, the computational efficiency of running microscopic traffic simulations to obtain performance evaluation results cannot support solving the SRSO problem in a timely manner to promptly respond to signals' failure. In existing literature, metamodels (or surrogate models) are proposed to address the tight computational budget issue in solving simulation-based optimization problems for transportation systems (Juan et al., 2015; Osorio and Bierlaire, 2013; Osorio and Chong, 2015; Osorio and Wang, 2017), although not for exactly the same research context. Generally speaking, metamodels (or surrogate models) are used to get an approximation of the objective function, such as total delay in the system, obtained by simulation. For instance, in Osorio et al.'s work, the metamodels leveraging the queueing network models are fitted to a set of simulated observations (Osorio and Chong, 2015; Osorio and Wang, 2017). Inspired by these existing metamodeling efforts, with the rapid developing of machine learning techniques, we are interested in exploring learning models' potential to server as a similar role, i.e., a metamodel (or surrogate model), for solving simulation-based optional sequence ordering problem, i.e., SRSO problem in this work.

Therefore, machine learning techniques are leveraged in this study to address the computational challenge in order to capture the dynamic system behavior in a timely manner. Based on the understanding that the traffic status of road sections—more specifically, movements at intersections—are closely related to each other if they are connected topologically, a Structural Recurrent Neural Network (SRNN) model (Jain et al., 2016) leveraging Spatio-temporal (ST) graph representation is used to capture the spatio-temporal interaction between adjacent movements among multiple intersections. A case study of the road network in downtown Boise, Idaho (a built-in example network in VISSIM) is conducted to demonstrate and verify the

effectiveness and efficiency of the proposed methodology. The selection of SRNN among various machine learning models is based on the following considerations. Firstly, transportation road network can be modeled as a directed graph and the topological information of the graph is helpful for modeling transportation system behavior and also for predicting the system performance. Secondly, the connection between adjacent movements is directional and the directional features matter while building up learning models in this research context. Thirdly, in the SRSO problem, the network structure is dynamic as there are both failure and restoration of signals at intersections. It is challenging to frame the learning model to capture the correspondent system dynamic behavior. More discussion on how SRNN could help us fully utilize the "features" (useful information to build up the learning model) to address these challenges of SRSO problem will be given in Section 3 after the comparative methodologies are reviewed in Section 2.

The remainder of this paper is organized as follows. Section 2 reviews the literature on related topics, including the resilience of transportation systems against cyber failure and learning-based performance prediction for the transportation systems. In this section, more detailed discussion on how SRNN serves better for the research purpose of this study will be given based on literature review. Section 3 presents the proposed learning based AATD prediction framework and the Structural Recurrent Neural Network (SRNN) model developed for solving this problem. Section 4 presents a case study to verify the effectiveness and efficiency of the proposed methodology. In this section, the significance of selecting proper signal restoration sequence is illustrated through two typical failure scenarios before the learning-based sequence ordering results are presented and evaluated. Different impacts of failure scenarios on system performance are further interpreted from a Macroscopic Fundamental Diagram (MFD) perspective in the appendix. Finally, key findings are summarized in the Conclusions, and the limitations of this study and future research directions to better solve the SRSO problem are also discussed.

2 Literature Review

2.1 Resilience of transportation system against cyber failure

Resilience, the concept introduced by Holling for ecological systems (Holling, 1973), has been studied widely in various fields and different contexts. It is usually defined as the ability of a system to retain the same functionality after a disruption and the capability of self-organization to the changes caused by a disturbance (Walker et al., 2002). Cyber failure is inevitable with the increasing number of cyber components involved in the monitoring and operation of modern Critical Infrastructure (CI) systems as a complex, integrated and evolving process (Guo et al., 2017). It is one of the most—if not the most—critical types of failure in a CI system, highlighting the importance of studying cyber failure impacts on system performance and the need for countermeasures to reduce these impacts. Various countermeasures can be implemented to improve the response of infrastructure systems to cyber failures, such as improving cyber components' adaptation to changes, improving the tolerance level of cyber components, and optimizing restoration efforts after disruptions (Mattsson and Jenelius, 2015).

Transportation is recognized as the third most vulnerable sector exposed to cyber-failure, according to a recent white paper released by Gallagher (Gallagher, 2018). As reported, there are at least 100,000 intersections in the US and Canada (Ghena et al., 2014), and 200,000 traffic sensors deployed worldwide that are exposed to cyber vulnerability (Cerrudo, 2015). Given the criticality of transportation systems to the functionality and efficiency of daily economic activities of a city, the U.S. Department of Transportation has developed the Cyber Security Evaluation

Program and Cyber Resilience Review Process to better assess the cyber security of transportation systems (DHS, 2015). Recently, there are some emerging literature modeling the potential impacts of cyber failures on transportation system performance. Reilly et al. studied freeway networks instrumented with coordinated ramp metering and the potential of well-designed antagonistic cyber-attacks targeting such control systems to induce arbitrarily complex congestion patterns in the system (Reilly et al., 2016). They discussed various types of cyber-attacks (e.g., direct physical access, virtual access) to transportation ramp metering management systems; however, how to enhance transportation system performance against cyber-attack is not mentioned in their work. Oricchio et al. also studied the effect of traffic signal malfunction—yellow/red (flash yellow on a major road and flash red on all other movements) or red/red (flash red on all approaches)—on the delay at intersections for vehicles on major and minor roads (Oricchio et al., 2008). Some existing literature studied signal priority and/or preemption, which can be considered a disturbance in traffic signal normal pattern and demonstrated its impact on travel cost (Mei et al., 2019).

It should be noted that most studies on the effects of signal failure were conducted at microscopic or mesoscopic level. For example, Reilly et al. (Reilly et al., 2016) applied a cell-transmission-model (CTM) with on-ramps modeled as queue buffers to examine the efficacy of control schemes from a cyber attacker's standpoint. Oricchio et al. conducted a simulation in VISSIM to obtain data for analyzing the impact of signal malfunction (Oricchio et al., 2008). A simulation-based system performance evaluation has been adopted widely for signal failure studies, as it provides the flexibility to model various signal failure patterns. Also, as the transportation system is a complex, nonlinear, dynamic system with various driver behaviors, vehicle types, and infrastructure geometries interweaving with each other, it is nearly impossible to get a closed-form formulation to capture the impact of signal failure on system performance (Osorio and Chong, 2015). Therefore, in this study, system performance under the context of signal failure is also evaluated through simulation. However, the performance evaluation based on simulation could not meet the time efficiency requirement to support online decision-making for prompt response after signal failure. Therefore, the existing literature on learning-based performance evaluation for transportation system is also reviewed, as noted in the next subsection.

In summary, although there are some recent research efforts on modeling the impacts of signal failures on transportation system performance, this problem has not been thoroughly studied. Also, it lacks signal failure-related transportation system resilience studies, especially from restoration planning perspectives. In this work, we focus on post-failure restoration of a transportation system—more specifically, the impact of restoration sequence of failed signals on transportation system performance—and propose a learning-based method to rank the optional restoration sequences for multiple failed signals.

2.2 Learning-based performance prediction for transportation system

Performance evaluation or prediction for a transportation system is the prerequisite for conducting effective and efficient traffic monitoring, management, and deploying practical control strategies. Traditional models, either parametric, such as Autoregressive Integrated Moving Average (ARIMA) (Shekhar and Williams, 2007) and Kalman filtering (Guo et al., 2014), or nonparametric, such as k-nearest neighbor (K-NN) method, Support Vector Regression (SVR), etc., are limited in accommodating a relatively large dataset in a systematic and flexible way with network-wide performance prediction as the target. Also, they do not have the capability to capture the topological information embedded in the transportation network, which is actually very helpful

and informative, as traffic flow is highly constrained by roadway structure and the traffic status of adjacent links are interacting with each other, both temporally and spatially.

The rapid development and widespread application of artificial intelligence, especially machine learning techniques, triggered by the increasingly powerful computing and storage capabilities, has attracted more and more research efforts on learning-based performance prediction for transportation systems. Observing the time-varying properties of traffic data, RNN was applied in various architectures to capture the time-scale interdependencies among traffic data with different gating mechanisms, such as Long Short-Term Memories (LSTM) (Ma et al., 2015; Zhang et al., 2017) and Gated Recurrent Unit (GRU) (Wu et al., 2018). RNN models are designed for modeling a temporal sequence using its internal state (memory) to process sequences of inputs with variable length (Abiodun et al., 2018; Dupond, 2019; Tealab, 2018), which makes them suitable for tasks such as unsegmented, connected handwriting recognition (Graves et al., 2009; Ho et al., 2008) or speech recognition (Li and Wu, 2015; Sak et al., 2014). Therefore, RNN models are appropriate to capture the time-scale interdependencies among traffic data. However, the RNN models lack the capability of modeling spatial interdependencies among multiple road sections or movements, not to mention representing the topological information in road networks that is very helpful and informative for performance evaluation or prediction of a transportation system as noted.

Recently, more efforts have focused on depicting the spatial features embedded in a transportation network to address the spatial interaction in traffic data. Existing works include the adoption of Convolutional Neural Network (CNN) (Lv et al., 2014; Ma et al., 2017; Zhang et al., 2017), capsule network (CapsNet) (Kim et al., 2018), Generative Adversarial Network (GAN), etc. However, instead of explicitly using the topological information—more specifically, upstream and downstream adjacency information—most existing works adopted spatial information in analogy with pixels in images (Ma et al., 2017). In this way, the learning methods developed for image processing, which is a major application area for machine learning, could be leveraged in a more straightforward way. However, these methods cannot fully use the topological information, which is very helpful to infer the spatio-temporal interactions among traffic data. Also, the computational complexity of these image-based methods increases along with the size of the network, which limits their scalability to large transportation networks (Kim et al., 2019).

Most recently, the spatio-temporal feature extraction keeping topological information to some extent is attracting more attention of researchers. Cui et al. applied a Graph Wavelet Neural Network (Xu et al., 2019) to capture the localized topological information to improve prediction accuracy. However, in Cui et al.'s work, the transportation networks are represented as an undirected graph consisting of vertices and edges representing sensing locations and connecting links, respectively, with graph wavelet operators acting as filters in the gates of the recurrent neural network (Cui et al., 2020). To capture the directional interactions, the SRNN method derived from spatio-temporal graphs as an effective approach for factor graph representation is adopted in several efforts recently (Kim et al., 2019); (Brendel and Todorovic, 2011; Jain et al., 2016; Koppula and Saxena, 2013). SRNN method can capture the spatial and temporal information explicitly in its feature extraction.

Road network can be represented as a directed graph under this SRNN methodological framework. More specifically, for the delay estimation at an intersection, the movement direction,

either in or out of the intersection, should be differentiated, which can be realized by applying SRNN method. In addition to the capability of capturing directional topological information explicitly, SRNN method has the potential to be tailored to build up the learning model for a road network with different types of nodes. This characteristic, which will be explained with more details in Section 3, is critical for achieving the goal of this research as there are two alternative modes of signals in the system, i.e. "normal" or "failed". Therefore, to address the challenges of capturing directional topological information and modeling various types of nodes in the system, our research modified the original SRNN method and applied it in solving the restoration sequence ordering problem.

3 Problem Statement and Research Approach

3.1 Problem statement

In this study, we assume that signal failure at a specific intersection causes all signal heads at that intersection to fail and, similar to a previous study (Oricchio et al., 2008), that signal failures make traffic signals go into the emergency state, namely the malfunctioning flash mode. The malfunctioning flash mode works functionally similar to stop signs following priority rules, which must be incorporated in the design of any signalized intersection, including both yellow/red manner (flash yellow on a major road and flash red on all other movements) and red/red manner (flash red on all approaches) in practice (Oricchio et al., 2008). Although the meaning of a yellow flash and a red flash is regulated by the legal code of each state, drivers are generally required to stop at a flashing red signal indication and to proceed with caution at a flashing yellow indication. Thus, in this work, we assumed that during flash mode, approaching vehicles from any direction make a stop and then follow priority rules to proceed. In reality, misunderstanding of the flashing mode may occur and lead to crashes, which could further deteriorate transportation network performance. However, in this study, we assume there is no such misunderstanding.

When a set of traffic signals fail (go into flash mode), we assume that, due to the limited number of traffic technicians, the signals can be fixed one by one following a restoration sequence. In reality, even when more traffic technicians are available for a larger area, they would be assigned to subareas of the network to repair signals in their assigned area. Therefore, within each subarea, the assumption that signals will be fixed one by one remains reasonable when focusing on subarea restoration planning. Therefore, this study aims to find a restoration sequence that results in less disruption to system performance caused by traffic signal failures. The Accumulated Total Delay (ATD), the total delay through restoration, used widely in the existing literature (Ganin et al., 2019) is adopted herein to evaluate signal failure impact on the performance of the corresponding intersection. Fig. 1 shows the pre-event, response, and recovery phases of a restoration process and also indicates the performance evaluation metric, ATD. The studied area consists of intersections with several movements at composing approaches. Therefore, the system level performance metric, Aggregated ATD (AATD), is defined as the aggregation of total delay in all movements in the studied area accumulated during the restoration process.

Although, given a specific restoration sequence, AATD could be calculated based on individual vehicle delay information simulated in microscopic simulation software such as VISSIM, the time efficiency of running simulations is not sufficient to support restoration sequence ordering in an online manner. Therefore, in this work, the SRNN method (Kim et al., 2019) is leveraged to predict system performance, i.e., AATD, during the restoration process, in the context of multiple signals' failure and restoration. This problem setting exposes extra

challenges, as the network status, i.e. traffic signal status, is interrupted and time varying. Although there are also randomness and uncertainty in the dataset collected for traffic flow status prediction, such as volume, speed, etc., for a normal transportation system, there are no severe interruptions to the network configuration in existing works. In this work, traffic signal failure can be viewed as an interruption to the node of the transportation network, which makes the network configuration unstable and predicting system performance thereafter even more difficult. Similarly, each restoration effort changing the signal status from failure back to normal status will trigger an "interruption" to the network configuration once again. Furthermore, to evaluate feasible restoration sequences, the total delay at each intersection at multiple consecutive time steps should be predicted, which makes it even more challenging to solve this problem effectively.

With historical traffic data, i.e., travel delay at movements, obtained through simulation, and the topological information expressed as an adjacency matrix, the objective of the learning-

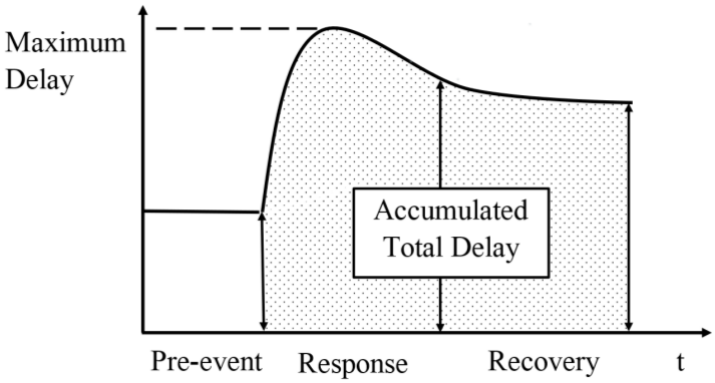

Fig. 1. Accumulated system performance measurement for restoration sequence ordering for multiple signals' failure

based approach is to predict the total travel delays at movements in consecutive time steps. In this research, as the signals could fail and then go back to normal after restoration, the signal mode could impact the movement status and eventually impact the interaction pattern between adjacent movements. Therefore, movement status should be taken into consideration in the learning model and the feature set extracted to feed into the learning model. Hence, the historical data includes not only the delay of each movement at intersections but also the signal status, i.e., corresponding movement status. The prediction for the consecutive time steps will be conducted under the circumstances with a given restoration sequence and the specified restoration time for each failed signal.

3.2 Research Approach

The overall framework of the proposed learning-based SRSO solution method is illustrated in Fig. 2. To capture the spatial-temporal features in the context of multiple signals' failure and restoration, a SRNN learning model is adopted to predict system performance under various restoration sequences. More specifically, the first step is to sample signal failure scenarios and then randomly select corresponding restoration sequences to generate the dataset. Then, the ground truth AATD for these selected restoration sequences are evaluated through simulation in VISSIM. The overall dataset is separated to serve different purposes, i.e. training, evaluation for delay prediction, and evaluation for ordering performance. For the training dataset, feature sets extracted from the simulation results are fed into the SRNN framework to train parameters of the model.

Then, the trained signal restoration sequence ordering model can be integrated with Genetic Algorithm to support the restoration sequences optimization eventually, as GA relies heavily on the ranking of optional sequences either generated as the first generation of solution or obtained through the selection, crossover, and mutation processes in the following up generations. In this work, we are focusing on building, training, and evaluating the SRNN model for the ordering of optional sequences, whereas leaving the integration of the SRNN based ordering model into the GA based sequence optimization to be future effort. More details of the proposed methodological framework are illustrated in the following subsections.

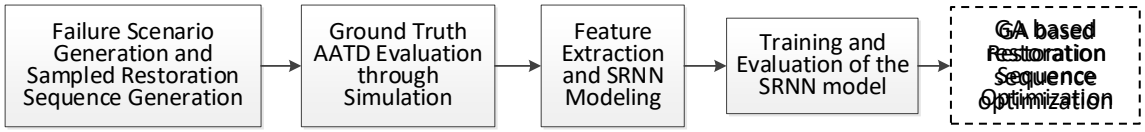

Fig. 2. Framework illustration of the proposed SRSO method

3.2.1 Introduction of Structural Recurrent Neural Network (SRNN) method

RNN architectures demonstrate remarkable capability in terms of modeling sequences that could be applied in natural language processing (Yin et al., 2017), image recognition (Lev et al., 2016), etc. However, traditional RNN cannot incorporate the spatio-temporal structure embedded in some other problems, as exemplified later (Jain et al., 2016). Spatio-temporal structures are both prevalent and of great help in solving learning problems, such as the recognition of interaction between human and environment, object trajectory prediction in video processing (Jain et al., 2016), and the performance prediction for systems with explicit spatio-temporal structure, such as transportation networks (Kim et al., 2019), etc. Therefore, the SRNN method was proposed by Jain et al. in 2016 to bridge the gap between traditional RNN methods and the effective use of spatio-temporal structure in learning problems. In a SRNN model, the connected components in a system of interest whose performance are going to be predicted or labels are pending to be recognized are modeled as nodes in a spatio-temporal (ST) graph. ST-graph is a type of factor graph (Kschischang et al., 2001) in which all the components, either nodes or edges, contributing to the performance prediction of the system represented by the graph are termed as "factors." Hence, the interactions between nodes in transportation system, either temporal or spatial, are represented by edges in the factor graph (Kschischang et al., 2001). Edges indicating temporal or spatial interactions are different types of edge factors. The Spatio-temporal (ST) graph could also have different types of node factors if there are different types of nodes in the system, such as human and objects in the recognition of interaction between human and environment problem (Jain et al., 2016). The SRNN model is designed to be applicable to various systems that could be represented by ST graphs (Jain et al., 2016); it is also demonstrated to be differentiable and scalable in the literature (Jain et al., 2016; Kim et al., 2019). Hence, it has been widely used in solving human action detection (Yan et al., 2018), visual question answering (Teney et al., 2017), human contact tracing in crowds (Vemula et al., 2018), and driver maneuver anticipation (Jain et al., 2016) problems.

3.2.2 ST graph representation for Aggregated Accumulated Total Delay (AATD) prediction

In this work, the original SRNN model is modified to predict the AATD in the system, which is the aggregation of the delay of all movements at studied intersections accumulated over the restoration process. More specifically, movements at intersections are modeled as nodes in the ST graph. As shown in Fig. 3, given a transportation network, each intersection is expanded to its

componential movements. Then, the interactions between movements, i.e., upstream and downstream adjacency, are modeled as spatial edges in the ST graph to capture the directed spatial interaction between movements, which is constrained by both the topology of the network and the intersection operation status, i.e., at normal mode or failure mode. As stated in Subsection 3.1, malfunctioning flash mode works functionally similar to stop signs following priority rules. The modified SRNN model, proposed in this work, can capture the different spatial interaction "patterns" under different "modes" of the componential movements associated with signals under normal or failed condition, by specifying the "mode" of the movement in the node feature extraction explicitly. Furthermore, the delay of one movement is also affected by the delay of this movement at the previous time step. Therefore, the temporal edges between nodes are used to model this impact in time scale.

More specifically, M is the set of movements in the network of interest, $|M| = N$. x_u^t denotes the delay of movement u at time step t, with $u \in M$. δ_u^t denotes the movement status which is a binary variable with 0 indicates normal mode and 1 indicates failure mode. Given time series of travel delay dataset $\{y_u^t\}$ and movement status dataset $\left\{\delta_u^t\right\}$ at time steps $t = t_c - l + 1, \ldots, t_c$ for all the movements $u = 1, 2, \ldots, N$, the travel delay at the next time step $y_u^{t_c+1}$ will be predicted, where t_c and l represent the current time step and the length of the historical data to be used for the prediction respectively. Similarly, the prediction could be rolled over to the following up time steps denoted as $y_u^{t_c+2}, y_u^{t_c+3}, \ldots$ with a given restoration sequence to be evaluated, i.e. given $\left\{\delta_u^t\right\}$ for the following up time steps.

Given the set of nodes, i.e., movements, denoted as M, the spatial edges are represented by the directed adjacency matrix A between connected nodes. For instance, u and v are two adjacent movements in the network. If traffic flow comes from movement u to movement v, then $A(u, v) = 1$ and $e_{(u,v)} \in \xi_s$, where $e_{(u,v)}$ is the edge directed from node u to node v in the network, and ξ_s is the spatial edge set in the network. As the ST graph is used to capture both spatial and temporal interactions, the spatially connected graph represented by $G = (M, \xi_s)$ is unrolled to the ST graph represented by $G_{ST} = (M, \xi_S, \xi_T)$, where ξ_T denotes the temporal edge set in the network. As noted, the delay of one movement is affected by the delay of this movement at the previous time step. The temporal edge $e_{(u,u)}^t$ directed from node u^{t-1} to node u^t is used to

model this impact in time scale. x_u^t denotes the feature of node $u \in M$ at time step t, i.e., the total delay of all vehicles experienced in movement u at time step t, with the delay of a specific vehicle calculated as the real travel time subtracting free flow travel time. In Fig. 3, both the spatial and temporal edges are labeled with the associated edge factors.

$\mathbf{x}_{(u,u)}^t$ is the feature set associated with the temporal edge $e_{(u,u)}^t$, which is used to implement the temporal impact from node u^{t-1} to node u^t in the SRNN model. $\mathbf{x}_{(u,u)}^t$ is also termed as "temporal edge factor" . More specifically, $\mathbf{x}_{(u,u)}^t = [x_u^{t-1}, x_u^t]$ is the concatenation of node features of node u at time step $t-1$ and node u at time step t. $\mathbf{x}_{(w,u)}^t$ is the feature set associated with the spatial edge $e_{(w,u)}^t$ which is used to implement the spatial impact from node w^t to node u^t in the SRNN model. Similarly, $\mathbf{x}_{(w,u)}^t$ is also termed as "spatial edge factor" and obtained by $\mathbf{x}_{(w,u)}^t = [x_w^t, x_u^t]$, i.e., the concatenation of node features of node w and node u at time step t. Thereafter, the spatio-temporal interactions between movements could be captured by the ST graph representation effectively. The modeling of transportation network as a ST graph is illustrated in Fig. 3, within which w is the upstream movement of movement u, whereas v is the downstream movement of movement u. Furthermore, in Fig. 3, the superscript t for each node is

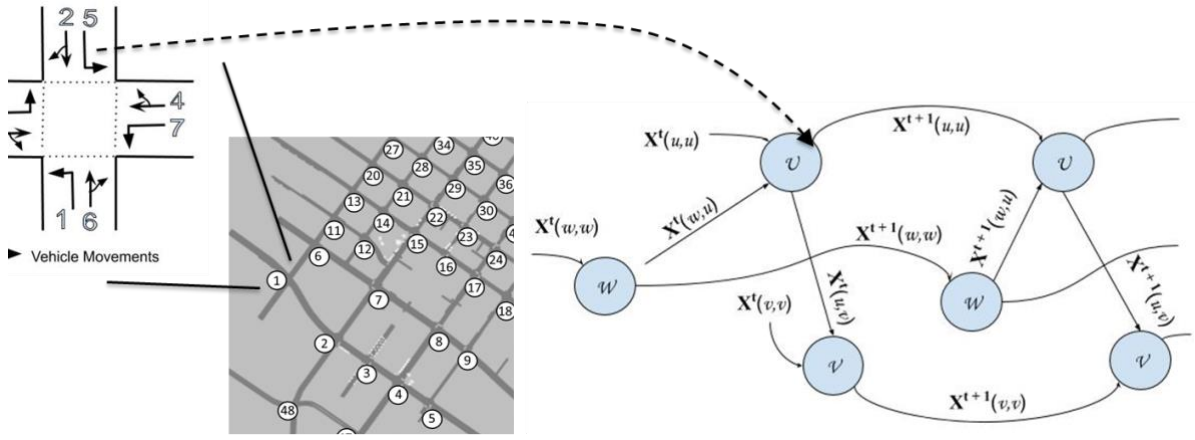

Fig. 3. Modeling the transportation network as a spatio-temporal (ST) graph. Each movement at an intersection corresponds to a node in the ST graph. The adjacent movements with traffic flow connecting each other are connected by spatial edges in the ST graph. The nodes representing the status of one movement at two consecutive time steps are connected by temporal edges in the ST graph. Note that the superscript t for each node is omitted for simplicity.

omitted for simplicity, i.e., u^t and u^{t+1} are not differentiated explicitly and are shown as two nodes connected by a temporal edge factor $\mathbf{x}_{(u,u)}^{t+1}$.

3.2.3 Modified SRNN model for AATD prediction

After extracting the ST graph representation and the associated feature sets for the studied transportation network, we modify SRNN model for AATD prediction so that it can be used to solve SRSO problem. Fig. 4 illustrates the SRNN framework for one movement performance prediction in the forward-path. It could be expanded to the SRNN model for multiple node

performance prediction according to its associated ST graph. The componential RNNs associated with the node factors are termed as "Node-RNNs" and denoted as $\mathbf{R}_M$. The RNNs associated with the spatial edge factors are termed as "Spatial Edge-RNNs" and denoted as $\mathbf{R}_{\xi_S}$. The RNNs associated with the temporal edge factors are termed as "Temporal Edge-RNNs", denoted as $\mathbf{R}_{\xi_T}$. LSTMs are used for all componential RNNs in the network; however, the Node-RNNs and Edge-RNNs could have different hyperparameter settings.

Take node u in Fig. 4 as an example. According to the adjacency matrix A, describing the network topology, there are two nodes v, w connected to node u. The spatial edges connected to node u is identified as $\square(u)=\left\{e^t_{(u,v)}\in\xi_S, e^t_{(w,u)}\in\xi_S\right\}$. The time series of node features, i.e., historical movement delay data $\left\{x^t_u\right\}^{t_c}_{t=t_c-l+1}$, $\left\{x^t_v\right\}^{t_c}_{t=t_c-l+1}$, $\left\{x^t_w\right\}^{t_c}_{t=t_c-l+1}$ are fed into this SRNN architecture to predict the total delay in movement u. Then, the edge features can be extracted according to Section 3.2.2 with associated combinations of $\left\{x^t_u\right\}^{t_c}_{t=t_c-l+1}$, $\left\{x^t_v\right\}^{t_c}_{t=t_c-l+1}$, $\left\{x^t_w\right\}^{t_c}_{t=t_c-l+1}$ and $\left\{x^{t-1}_u\right\}^{t_c}_{t=t_c-l+1}$. After extracting node features and edge features, the spatial edge features are fed into the Spatial Edge-RNN, whereas the temporal edge features are fed into the Temporal Edge-RNN. Then, the node features are concatenated together with hidden states of the Temporal Edge-RNN, hidden states of the Spatial Edge-RNN, and the movement status (failure or normal), to be fed into the Node-RNN to predict the node performance, i.e., total delay for this movement. The introduction of movement status makes it possible to capture two different modes of movements, i.e. normal or failed. As noted, the spatial interaction pattern among movements is different under different mode, which can be modeled by the modified SRNN model. It is worth mentioning that the modeling framework shown in Fig. 4 for movements are not isolated, but connected with each other according to the ST graph shown in Fig. 3. In this way, all nodes in the system are connected and their spatial-temporal interactions are modeled so that eventually the AATD can be predicted as the aggregation of total delay in all movements in the studied area accumulated during the restoration process.

Similar as Kim et al.'s work (Kim et al., 2018), in our study, the modified SRNN model integrates the node and edge features of target nodes nonlinearly to predict the performance of the target nodes. However, the integration of movement status is unique for this post disruptive event SRSO problem. Moreover, we extend one step prediction to the prediction for several consecutive time steps in this study. More details regarding the components of the SRNN architecture for the forward path are introduced as follows. The loss function and backward propagation are introduced in the next subsection.

1) *Input features' embedding layer*

Determined by the network topology, there could be different length of feature sets as inputs for Node-RNNs or Edge-RNNs of different nodes in the network. To obtain fixed-length vectors as inputs to the RNNs, embedding functions are applied as a linear transformation of the original input features, denoted as $\phi(\cdot)$. More specifically, it is implemented as a linear layer with a rectified linear unit (ReLU) activation and dropout.

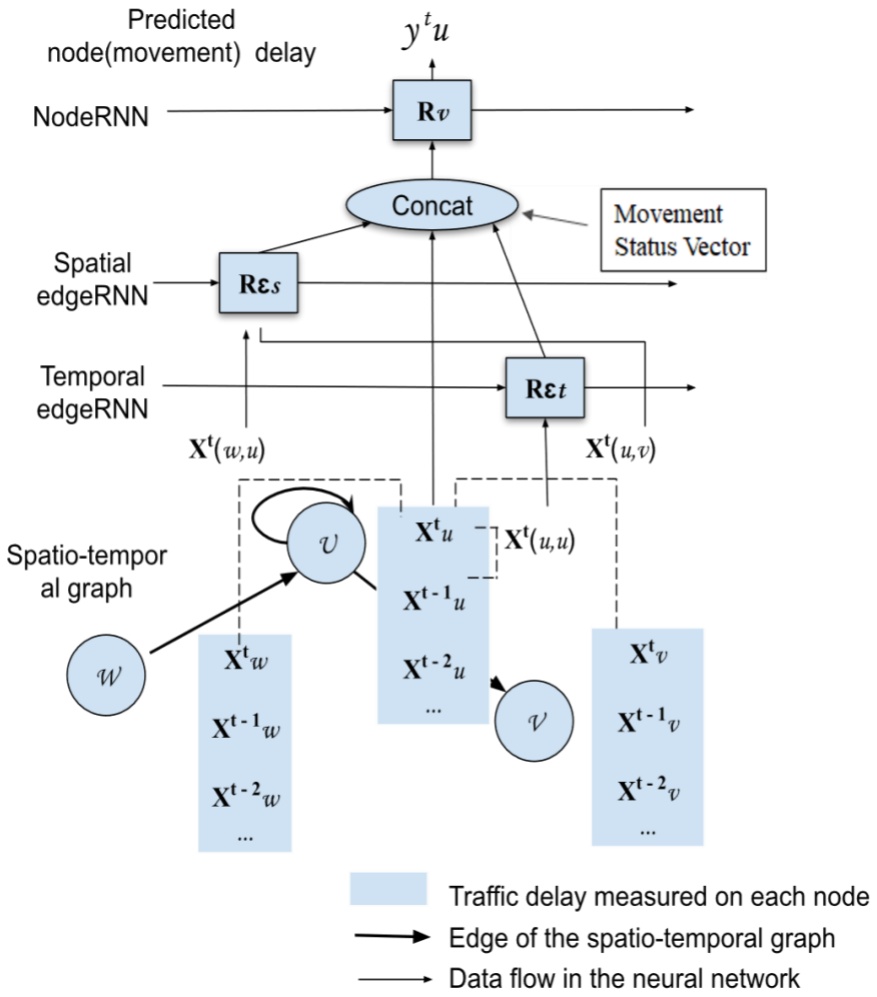

Fig. 4. Modified Structural Recurrent Neural Network framework for one movement performance (total delay) prediction in the forward path

2) Spatial Edge-RNN

The size of the Spatial Edge-RNN, denoted as λ_{ξ_S}, is configurable as a hyperparameter to fine-tune the SRNN model. In addition to the spatial edge features $\left\{\mathbf{x}_e^t\right\}_{e\in\xi_S}$, the hidden states of the Spatial Edge-RNN at time step $t-1$, h_S^{t-1}, with a dimension of $|\xi_S|\times\lambda_{\xi_S}$ are also fed into the Spatial Edge-RNN. The spatial edge features $\left\{\mathbf{x}_e^t\right\}_{e\in\xi_S}$ are converted into a fixed length vector $\mathbf{a}_S^t$ as output of the embedding layer. Then, $\mathbf{a}_S^t$ is concatenated with h_S^{t-1} to be fed into the LSTM cell. In this way, the time-scale impact is also captured by the connection between LSTM cells of consecutive Edge-RNNs.

$$\mathbf{a}_S^t = \phi\left(\left\{\mathbf{x}_e^t\right\}_{e\in\xi_S}; W_S^E\right) \tag{1.1}$$

$$h_S^t = \mathrm{LSTM}\left(\mathbf{a}_S^t, h_S^{t-1}; W_S^L\right) \tag{1.2}$$

where W_S^E and W_S^L are the weights of the embedding layer and the LSTM cell, respectively.

3) Temporal Edge-RNN

Similarly, for the Temporal Edge-RNN, the temporal edge features are fed into the embedding layer and resulting in a fixed length vector $\mathbf{a}_T^t$. Then, it is concatenated with h_T^{t-1} to be fed into the LSTM cell, where h_T^{t-1} has the dimension of $|\xi_T| \times \lambda_{\xi_T} = 1 \times \lambda_{\xi_T}$ with λ_{ξ_T} denoting the size of the Temporal Edge-RNN that is also configurable. Actually, $|\xi_T| = 1$, as for each node, there is one temporal edge representing the impact from its previous time step, which is also illustrated in Fig. 3.

$$\mathbf{a}_T^t = \phi\left(\left\{\mathbf{x}_e^t\right\}_{e \in \xi_T}; W_T^E\right) \tag{1.3}$$

$$h_T^t = \mathrm{LSTM}\left(\mathbf{a}_T^t, h_T^{t-1}; W_T^L\right) \tag{1.4}$$

where W_T^E and W_T^L are the weights of the embedding layer and the LSTM cell for the Temporal Edge-RNN respectively.

4) Node-RNN

In addition to the node features, the Node-RNN also takes the hidden states and the outputs of the Spatial Edge-RNN and the Temporal Edge-RNN as inputs.

Given each node $u \in M$, the spatial edges connected to it are identified as $\square(u)$. Then, the corresponding rows of the hidden state matrix of the Spatial edge-RNN are extracted as $h_{\square(u)}^t = h_S^t\left(\square(u)\right)$ with the dimension of $|\square(u)| \times \lambda_{\xi_S}$. A row vector of the hidden state of the Temporal Edge-RNN associated with node u denoted as $h_{T_u}^t$ is also going to be fed into the model. Then, the row vectors of $h_{\square(u)}^t$ are aggregated to get the spatial edges' total contribution to the Node-RNN, which is calculated as:

$$h_{S_u}^t = \mathrm{sum}\left(h_S^t\left(\square(u)\right)\right) \tag{1.5}$$

The motivation to conduct this aggregation is two-fold. First, converting the $h_{\square(u)}^t$ with dimension $|\square(u)| \times \lambda_{\xi_S}$ to $h_{S_u}^t$ with dimension $1 \times \lambda_{\xi_S}$ facilitates the follow-up concatenation with $h_{T_u}^t$ that has dimension $1 \times \lambda_{\xi_T}$. Second, with the objective defined as predicting total delay of the studied movement, the connected movement with higher total delay has a more significant impact on the studied movement, and the total number of movements connected to the studied movement also matters. Therefore, the aggregation of spatial impacts of all the connected movements is more reasonable compared to taking the average of the spatial impacts.

Then, $h_{T_u}^t$ and $h_{S_u}^t$ are concatenated to $H_u^t = \text{concat}\left(h_{T_u}^t, h_{S_u}^t\right)$ with dimension of $1\times\left(\lambda_{\xi_T}+\lambda_{\xi_S}\right)$. The row vectors for all nodes in the node set M are vertically concatenated to serve as the input to the Node-RNN, denoted as H^t, representing the impact of spatio-temporal edges to the node performance prediction. The node feature, $\left\{x_u^t\right\}_{u\in M}$, the concatenated hidden state, H^t, and the movement status variable $\left\{\delta_u^t\right\}_{u\in M}$, are fed into the embedding layer and converted to a fixed-length vector to be sent to the LSTM cell as follows.

$$\mathbf{a}^t = \phi\left(concat\left(\left\{x_u^t\right\}_{u\in M}, \left\{\delta_u^t\right\}_{u\in M}\right); W^E\right) \tag{1.6}$$

$$\mathbf{a}_H^t = \phi\left(H^t; W_H^E\right) \tag{1.7}$$

$$h^t = LSTM\left(concat\left(\mathbf{a}^t, \mathbf{a}_H^t,\right), h^{t-1}; W^L\right) \tag{1.8}$$

$$\left\{y_u^t\right\} = W^O h^t \tag{1.9}$$

where W^E and W_H^E are the weights of the embedding layer for the node features and that for the concatenated hidden state respectively. W^L is the weight of the LSTM cell for the Node-RNN. The hidden state of the LSTM cell is the input of the linear output layer with weight W^O. The output of this final layer is the prediction for each node, i.e., predicted delay of movements, $\left\{y_u^t\right\}$ More specifically, $\left\{y_u^t\right\}$ is the predicted total delay for movement u based on all the information available at time step t. Therefore, $\left\{y_u^t\right\}$ is actually for the next time step $t+1$.

3.2.4 Loss function and backward propagation of the SRNN model for AATD prediction

After recording the total delay for each movement at each time step during the restoration process which is evaluated through simulation, the node features and edge features are extracted according to Subsection 3.2.2. Then, all these features go through the forward path explained in Subsection 3.2.3, with $\left\{y_u^t\right\}$ as the output of the forward path, i.e., the predicted total delay for movement u for the time step $t+1$ based on all the information available until time step t. Therefore, the prediction error is calculated according to the difference between $\left\{x_u^{t+1}\right\}, \left\{y_u^t\right\}$, where $\left\{x_u^{t+1}\right\}$ is the ground truth evaluated through data collected from simulation. More specifically, Mean Squared Error (MSE), i.e. SE averaged over all the movements in the studied area, is adopted as the loss function to be backpropagated in the training phase which is calculated as follows:

$$\text{MSE} = \frac{1}{N}\sum_{i=1}^{N}\left(x_i^{t+1} - y_i^t\right)^2 \tag{1.10}$$

During the training phase, the errors in prediction are back-propagated through the Node-RNN, the Spatial Edge-RNN, and the Temporal Edge-RNN involved in the forward-path (Jain et al., 2016). The trainable parameters of this SRNN model, summarized as $\left\{W_S^E, W_S^L, W_T^E, W_T^L, W^E, W_H^E, W^L, W^O\right\}$, will be optimized in the training phase through the Stochastic Gradient Descent (SGD) method. SGD is a stochastic approximation of gradient descent optimization. It replaces the actual gradient calculated from the entire data set by an estimate

548 calculated from a randomly selected subset of the data (Bottou, 1998), which helps reduce the
549 computational burden (Sra et al., 2012).

550 To support restoration sequence ordering, multiple time step performances are predicted
551 and then aggregated to be the prediction of the AATD in the system following a given restoration
552 sequence. In addition to the prediction loss measured by MSE, another evaluation metric is
553 proposed in terms of the ordering of various feasible restoration sequences, defined and explained
554 in Section 4 along with the case study.

555 In summary, the proposed modeling framework applies Spatial Edge-RNN and Temporal
556 Edge-RNN to model the spatial and temporal interactions, respectively. The node and edge
557 features integrated with the movement status are fed into the trained learning model to predict the
558 target node performance nonlinearly. Then, the system-level performance is aggregated through
559 all movements and all the time steps during the restoration process for each given restoration
560 sequence. The case study in Section 4 further demonstrates the effectiveness of the proposed
561 feature extraction based on the ST graph, the modified SRNN modeling framework, and the
562 learning-based sequence ordering method. In the following up work, the predicted system-level
563 performance AATD can be utilized to support the GA based restoration sequence optimization.

564 **4 Case Study**

565 The proposed methodology is applied to a case study network to demonstrate its effectiveness and
566 efficiency. The configuration of the case study network is presented, and the importance of
567 selecting proper restoration sequence is illustrated through two typical failure scenarios in
568 Subsection 4.1 and 4.2. The performance of the proposed SRNN model on predicting the AATD
569 in the case study network and on supporting the restoration sequence ordering is evaluated in
570 Subsection 4.3.

571 **4.1 Case study network configuration**

572 A case study of downtown Boise, Idaho (see Fig. 5(a)) is performed to demonstrate the proposed
573 research approach and solution algorithm. The transportation network of downtown Boise is a
574 built-in example in VISSIM with the input data, including lane configurations, volume inputs and
575 routing, signal timings, and model settings, collected based on real field information and provided
576 by local agency, i.e. Ada County Highway District (ACHD). This Boise case study network was
577 calibrated by ACHD based on the volume estimates provided by COMPASS and the average travel
578 times that were measured in the field. The network contains both regular and irregular grid-shaped
579 road networks with multiple road types such as principal arterials, minor arterials, and major
580 collectors (see Fig. 5(b)), with different traffic volumes and patterns at each intersection. The
581 classification of roads is retrieved from Idaho's statewide road system map (Waze-Maps, 2018),
582 which follows road functional classification defined by the Federal Highway Administration
583 (FHWA, 2013). A sub-area of downtown Boise, as shown inside the blue dashed line in Fig. 5(a),
584 is chosen as the region prone to signal failure and it consists of 19 intersections. As the impact of
585 the failed signal could propagate in the system, system performance is evaluated for a larger area
586 inside the red dashed line, which includes 34 intersections, with 135 movements in total connecting
587 the road sections between intersections.

588 For all signalized intersections, the VISSIM Ring Barrier Controller (RBC) module is used
589 to control signals, and signal timings are predefined in the built-in example according to the
590 calibrated model based on the real field collected data. Unsignalized intersections in the network

591 are regulated by stop signs and priority rules. Traffic flow injecting patterns for nodes at the
592 boundary of the network and the turning proportions of the traffic flow at each intersection are
593 predefined according to the calibrated model for the Boise downtown area.

594 In VISSIM simulation, once a signal fails, the control mode at the affected signalized
595 intersection changes to flashing mode, acting as priority rules, which changes the signalized
596 intersection into a four-way stop intersection. These priority rules in VISSIM prevent conflicts in
597 traffic by letting vehicles move only if a gap exists between them. A minimum of 3-second gap
598 time and 16.4 feet (5 m) distance were set for priority rules in this case study. It is also worth
599 mentioning that the driver behavior setting in VISSIM prevents drivers from occupying
600 intersections when there is congestion ahead, which guarantees the movement of other approaches
601 at that intersection.

(a) (b)

Fig. 5. (a) Simulation network in VISSIM for case study (subarea indicated by dashed line – red = area for system performance evaluation, blue = region prone to signal failure);
(b) downtown section of Boise, with road types represented by different colors – red = principal arterials, green = minor arterials, purple = major collectors.

602 Road sections between intersections are connected by movements at adjacent intersections.
603 In VISSIM, delay is defined as the travel time increase caused by the difference between desired
604 speed and actual speed. Note that the desired speed is the maximum free-flow speed allowed under
605 the imposed speed limit. To calculate the delay, a time step is specified, and the distance traveled
606 in that time step under actual speed is recorded. Thereafter, the time it takes a vehicle to travel that
607 recorded distance at the desired speed is calculated. The difference between these two times is the
608 vehicle delay. Total delay at a movement is the aggregation of the delay experienced by vehicles
609 that are moving in this movement during the evaluation time interval. Total delay in the studied
610 area is calculated as the sum of total delays of all movements in that area.

611 The simulation is started with 20 minutes of warm-up followed by 30 minutes of all signals
612 functioning properly; these first 50 minutes are identical in the simulation for different restoration
613 sequences. At the end of the 50 minutes, for a given failure scenario, all chosen intersections are
614 failed simultaneously. It is assumed that the time needed to repair a failed signal is 20 minutes in
615 this case study; therefore, the simulation ran for 20 minutes before one failed signal is restored,

and the failed signals are restored one by one following the restoration sequence. Therefore, the total simulation time varied with respect to the number of failed signals. For example, for a scenario with 4 signals failed, the total simulation time is 150 minutes; for a scenario with 6 signals failed, the total is 190 minutes. The time interval for data collection in VISSIM to evaluate system performance is 10 minutes. Accordingly, the total delay for each movement is predicted for every 10 minutes following a given restoration sequence in Subsection 4.3.

4.2 Empirical analysis to demonstrate the importance of restoration sequence optimization

Two failure scenarios with six signals failed are studied—Scenario I [2,6,7,13,14,16] and Scenario II [2,7,8,13,14,24]—to demonstrate the importance of restoration sequence optimization empirically. For Scenario I and Scenario II, 290 restoration sequences are randomly selected and multiple runs of each restoration are simulated in VISSIM to obtain performance evaluation outcomes. Total delay curves of these restoration sequences for these two scenarios are shown in Fig. 6(a) and Fig. 6(b). Observations based on the total delay curves of the case study are summarized as follows:

- Depending on the layout of the failed signals, the combinations of the same number of failed signals could lead to significantly different network performance during restoration. As shown by comparing Figs. 6(a) and 6(b), a large portion of restoration sequences for Scenario II leads to more delay than those for Scenario I. This observation is further interpreted in the appendix from a Macroscopic Fundamental Diagram point of view.
- There is a set of restoration sequences that can help dissipate congestion in the system after signal failure and reduce the AATD in the restoration process effectively. The restoration sequences with worse performance result in a highly congested network with much higher delay curves for both failure scenarios.

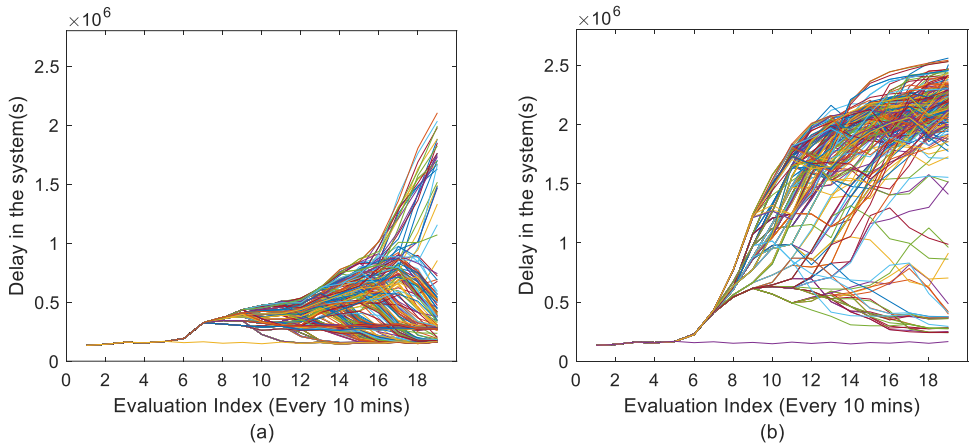

Fig. 6. Total delay curves under various traffic signal restoration sequences for two scenarios with six signals failed—(a) Scenario I [2,6,7,13,14,16] and (b) Scenario II [2,7,8,13,14,24] .

The first observation demonstrates the importance of following optimized or near-optimal restoration sequences to avoid cascading failure and gridlock in the network. However, a set of restoration sequences can help achieve this goal, referring to the second observation. As achieving the global optimal is computationally expensive, the research objective is set up to be achieving

near-optimal solutions in a timely manner for this study. Although inevitably there is error between the AATD predicted by the learning model and that obtained through running simulation, the predicted performance could result in restoration sequences leading to near-optimal solutions which still can solve the SRSO in a cost-efficient way with "good enough" restoration performance. As stated in *Ordinal Optimization* (Ho et al., 2008), "To quickly narrow the search for optimum performance to a 'good enough' subset in the design universe is more important than to estimate accurately the values of the system performance during the process of optimization." This statement is not only for the design of systems but also is applicable for the operational stage. Therefore, the concept of Ordinal Optimization is borrowed to evaluate the performance of the learning-based SRSO problem solution in Subsection 4.3.3.

4.3 Evaluation of SRNN-based AATD prediction and restoration sequence ordering

4.3.1 Data preparation and simulation-based ground truth performance evaluation

For the studied network shown in Fig. 5, the total delays of 135 movements composing 34 intersections are predicted according to the SRNN model illustrated in Section 3. The historical data length is set to be 3 in the SRNN model ($l = 3$), i.e., the total delays of the 135 movements of the previous 3 time-intervals are used to predict the total delays of the 135 movements in the following time interval. The training dataset is composed of failure scenarios with 2, 3, or 4 signals failed simultaneously. All combinations of two-signal failure for the 19 intersections prone to signal failure are enumerated with all feasible restoration sequences evaluated through simulation. For failure scenarios and restoration sequences with three or four signals failed, a subset of scenarios and restoration sequences are generated randomly. In total, the generated feasible restoration sequences are evaluated through simulations and served as the dataset with ground truth information. More specifically, 9975 pairs of $\left(\mathbf{X}, \hat{\mathbf{Y}}\right)$ are taken as the training dataset, 3255 pairs as the evaluation dataset, and 9765 pairs as the ordering performance evaluation dataset, with $\mathbf{X}$ indicating the input feature set obtained through the historical movement delay data with length $l = 3$ and $\hat{\mathbf{Y}}$ indicating the ground truth of the output of the model, i.e., total delays at 135 movements evaluated by running simulation in VISSIM. That is, the dataset and its corresponding scenarios used for the training, evaluation, and ordering performance evaluation purposes are different from each other. The overall input delay data are scaled to range [0, 1] before feeding into the learning model. The adjacency matrix between the movements of interest and the ST graph are extracted according to Subsection 3.2.2

4.3.2 SRNN model configuration

The SRNN learning model is built up according to Subsection 3.2.3. All componential RNN networks adopt the MSE loss function and Stochastic Gradient Descent (SGD) optimizer.

Based on grid search results compared for different settings, the following hyperparameters' setting is selected for further investigation. The size of the Node-RNNs and the Edge-RNNs are all set to be 32, and the gradient clipping value is set to be 5. The exponential decay rate for the optimizer is 0.99, and the dropout rate is 0.5. Then, the learning rate of the model is further fine-tuned using two strategies, i.e., step-based adjustment Step-LR and Cosine-Annealing-LR, as the learning rate has significant impact on the performance of the model trained. The implementation of the SRNN model refers to the model developed in the literature (Kim et al., 2019; Vemula et al., 2018). In the Step-LR strategy, the learning rate decays exponentially with the index of epochs, which could also be set to keep the same for several consecutive epochs.

For the Cosine-Annealing-LR, the learning rate changes as a cosine function with the index of epochs, with the cycle of the cosine function and the maximum and minimum learning rate configurable. The performance of these two fine-tune strategies for learning rate is also presented and compared in the next subsection.

4.3.3 Results Analysis

The performance of the proposed SRNN model on predicting the AATD in the case study network and on supporting the restoration sequence ordering is evaluated in this subsection.

As MSE is adopted as the loss function for backpropagation, Root Mean Squared Error (RMSE) is used as the loss to be aggregated through batches to obtain the average performance metric for each epoch, calculated as follows:

$$\mathrm{RMSE} = \sqrt{\frac{1}{N}\sum_{i=1}^{N}\left(x_i^{t+1} - y_i^t\right)^2} \tag{1.11}$$

In addition to the RMSE indicating prediction accuracy, ordering performance metrics, P_1, P_2 and L_1, L_2 are introduced as follows borrowing the idea from Ordinal Optimization. We denote the set of the top $k\%$ of the given sequences identified by the predicted AATD derived by the SRNN model as $I^*_{k\%}$, whose predicted AATD fall into the lowest $k\%$ of all the given sequences to be ranked. Whereas the set of the top $q\%$ of sequences identified by the real AATD according to the simulation results is denoted as $\hat{I}_{q\%}$. The two parameters $k\%$ and $q\%$ can be configurated in different settings to have different ordering performance metrics. The ordering performance evaluation metrics in our case study are defined as follows. P_1 indicates the possibility of the predicted top $k_1\%$ sequences overlapping with the real top $q_1\%$ sequences. P_2 indicates the possibility of the predicted top $k_2\%$ sequences overlapping with the real top $q_2\%$ sequences. Then, the length L of the intersection between $I^*_{k\%}$ and $\hat{I}_{q\%}$ is defined as follows to futher quantify the ordering performance.

$$L_1 = \left|I^*_{k_1\%} \cap \hat{I}_{q_1\%}\right|, \quad L_2 = \left|I^*_{k_2\%} \cap \hat{I}_{q_2\%}\right| \tag{1.12}$$

In the case study, for the ordering performance evaluation dataset, i.e. 9765 pairs of $\left(\mathbf{X}, \hat{\mathbf{Y}}\right)$, there are 651 sequences (each sequence has 15 pairs of data) evaluated first through simulation, then based on the learning model trained. We randomly sample 336 sequences from these 651 sequences for 400 times. Then, P is evaluated by the frequency of the predicted top $k\%$ sequences overlapping with the real top $q\%$ sequences among 400 samples. The length L of the intersection between $I^*_{k\%}$ and $\hat{I}_{q\%}$ is calculated as the average L over all 400 samples.

Fig. 7 shows the RMSE for the training and evaluation phase in each epoch which is firstly aggregated over all movements, and then averaged over the batches in the corresponding epoch. Note that the AATD aggregated over all movements and then averaged over all the simulations is 6.3607×10^4 s. Therefore, the RMSE converging to around 1000 s corresponds to less than 2% error. Another observation is that Step-LR results in a relatively consistent decreasing loss curve. Whereas, the Cosine-Annealing-LR strategy leads to fluctuating loss with the overall declining

trend of the loss curve. This is consistent with the expectation as the Cosine-Annealing-LR strategy is designed with the learning rate changing as a cosine function on purpose to help the model exit a local minimum and continue exploring the loss landscape. Therefore, compared to Step-LR, the Cosine-Annealing-LR strategy can help further reduce the loss at the cost of sacrificing the performance of some intermediate epochs. Then, $k_1\% = 6\%, q_1\% = 10\%$ and $k_2\% = 4\%, q_2\% = 8\%$ are set for the ordering performance evaluation in this case study. P_1 and P_2, for each epoch under Step-LR and Cosine-Annealing-LR tuning strategies are shown in Fig. 8. Note that, the performance of the Step-LR strategy converges around Epoch 60, whereas the performance of Cosine-Annealing-LR strategy can be further improved with more epochs of training and converges around Epoch 100 in our experiments. However, to make a fair comparison between these two strategies, the results from Epoch 1 to Epoch 71 is illustrated and compared. For the Step-LR strategy, the best performance is obtained from Epoch 66, with $P_1 = 1, P_2 = 1, L_1 = 8.125, L_2 = 4.882$; whereas the Cosine-Annealing-LR strategy performs best at Epoch 69, with $P_1 = 1, P_2 = 1, L_1 = 9.19, L_2 = 5.05$. Meanwhile, the $RMSE_{eval} = 869.125$ obtained by the Cosine-Annealing-LR strategy at Epoch 69, is much lower compared to $RMSE_{eval} = 1015.868$ obtained by the Step-LR strategy at Epoch 66.

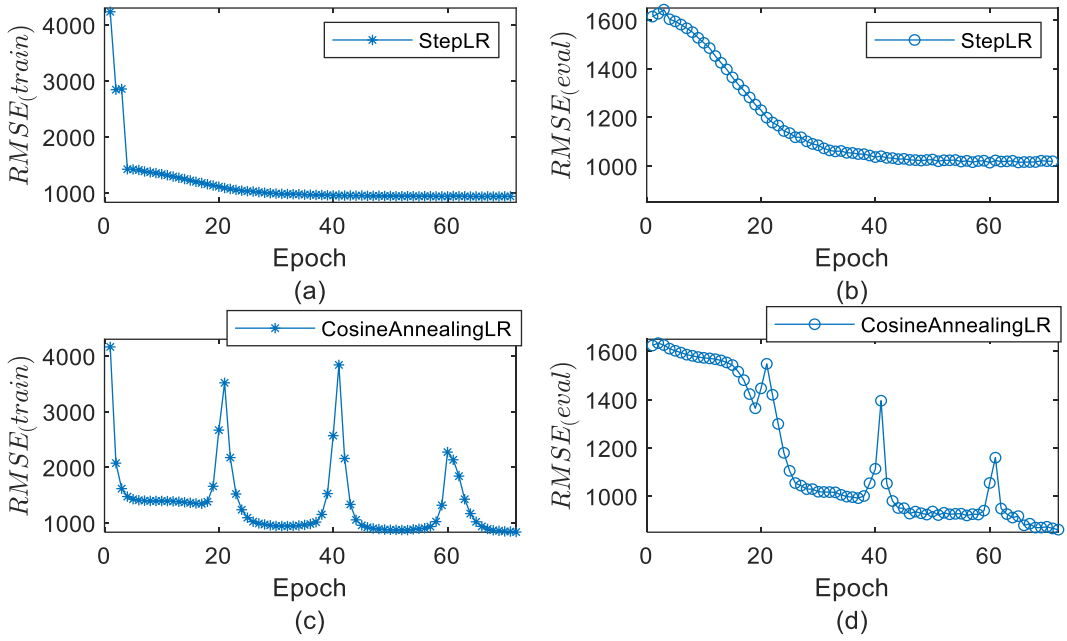

Fig. 7. RMSE for the training and evaluation phase in each epoch

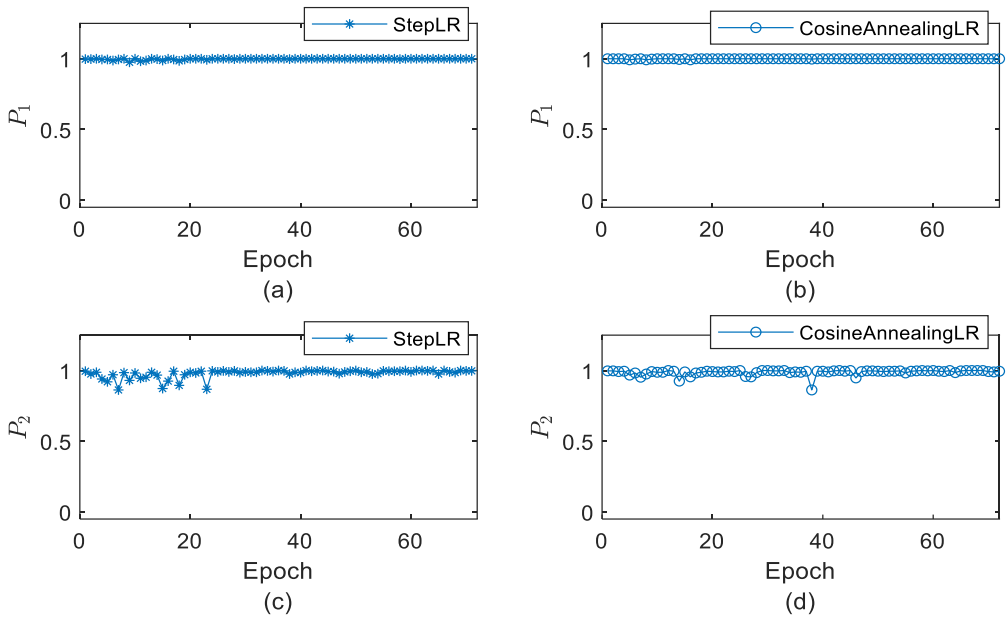

Fig. 8. P_1 and P_2 for each epoch under Step-LR and Cosine-Annealing-LR tuning strategies

To quantify the performance of the sequence ordering based on estimated AATD, we propose an evaluation metric, $Diff_{AATD}$ and conducted a test to compare the performance of Step-LR and Cosine-Annealing-LR strategies. All the restoration sequences in this test have real AATDs from simulation and estimated AATDs from learning based method. The restoration sequences are ordered according to real (simulated) AATDs and estimated AATDs respectively, which we call them Order 1 and Order 2. Note that in these two orders, the restoration sequences at same position, e.g. No. 10 in Order 1 and 2 could be different from each other. The metric $Diff_{AATD}$ is calculated as the difference between the real AATDs of the restoration sequences at same positions of the two orders and divided by the real AATD of the restoration sequence in Order 1 (see below 1.13). For simplification purpose, the superscript indicting the position of the restoration sequence is omitted in the equation.

$$Diff_{AATD} = \frac{\left| AATD_r - AATD_e \right|}{AATD_r} \tag{1.13}$$

Furthermore, the cumulated $Diff_{AATD}$ of the 50th, 65th, and 75th percentile of restoration sequences followed Step-LR and Cosine-Annealing-LR strategies are computed and listed in Table 1. It is observed that, for 75% of the evaluated sequences, the Cosine-Annealing-LR strategy can identify the restoration sequences with AATD performance approximate to the optimal solution identified by simulation results, with less than 0.71% performance difference, which is much better than the Step-LR strategy.

Table 1. Performance difference between sequences ordered by the real and estimated AATDs

Metrics	Step-LR	Cosine-Annealing-LR
50th Percentile of $Diff_{AATD}$	0%	0%

65th Percentile of $Diff_{AATD}$	0.38%	0%
75th Percentile of $Diff_{AATD}$	49.87%	0. 71%

In summary, the Cosine-Annealing-LR strategy leads to both lower loss value, better ordering performance, and shorter delay experienced in the restoration process compared to the Step-LR strategy.

5 Conclusions

Recognizing the significance of a resilient traffic management system against traffic signal failure, this study proposes a learning-based performance evaluation method to support the post-event optional restoration sequence ordering. The need to capture the dynamic behavior of a system in a timely manner limits the use of traditional simulation-based system performance evaluation during the online decision-making process. In the proposed method, simulation is used to obtain the ground truth performance evaluation in the data preparation phase. In the context of restoration, system performance is disrupted by the failure of control signals, which exposes an extra challenge to predict system performance effectively and efficiently. Observing the importance of capturing spatial-temporal interactions between movements in the roadway system, the SRNN leveraging the ST-graph representation of complex systems is adopted. Furthermore, the movement feature representation and its integration to the SRNN model are proposed in our study to help address the challenges. Specifically, the hyperparameter of the model, learning rate, is fine-tuned according to Step-LR and Cosine-Annealing-LR strategies.

A case study in downtown Boise leveraging a built-in model in VISSIM is conducted to exemplify the effectiveness and efficiency of the proposed methodology and reveals that the signal restoration sequence could impact system performance during and after the restoration process significantly. Furthermore, both AATD prediction accuracy and the performance of restoration sequence ordering are evaluated for the case study network. Outcomes show that the proposed methodology can effectively identify restoration sequences with less total delay experienced in the restoration process, i.e., AATD, ranked in top 8% of optional sequences in reverse order referring to ground truth information. Furthermore, in terms of the fine-tune of the learning rate, the Cosine-Annealing-LR strategy leads to both lower loss value, better ordering performance, and shorter delay experienced in the restoration process, compared to the Step-LR strategy.

It is worth mentioning that this study made an assumption that signals were fixed one by one, and the experiments and results analysis were based on that assumption. Such an assumption can be relaxed to allow multiple teams act simultaneously. On one hand, by partitioning the service area into subareas, the proposed methodology can still be used to solve the SRSO problem in each subarea. On the other hand, the learning-based performance evaluation is extendable to the circumstances with multiple teams act simultaneously. To further evaluate the performance of the proposed methodology under these generalized settings is part of our future work plan.

Limited by the functions and setting of the simulation tool that we used in this study, some scenarios that may occur in the real world during post-failure could not be reflected in the simulation, e.g., demand change due to trip cancellation based on real-time traveler information, vehicle rerouting, possible human interference with policemen deployed to congested intersections to direct traffic, etc. In future research, if a more powerful simulation platform is available,

researchers may include these scenarios in the study. In addition, in the future work, the system-level performance AATD predicted through learning model can be utilized to support the GA based restoration sequence optimization. Furthermore, in real application, given traffic patterns varying from peak-hours to non-peak hours, more simulations with different signal failure start times need to be performed to train different learning-based models for determining optimal restoration sequences for different time periods of the day. Moreover, due to limited field data collection under signal failure and restoration circumstances, the case study in this work is based on microscopic simulation. Further investigation and evaluation of the proposed methodology based on field collected data will also be of great interest with more and more data source becoming available in the future. Last but not least, as there is a vast literature of MFD based traffic signal control methodologies, working either in a modeling or a data-driven manner (Mercader and Haddad, 2021; Ren et al., 2020; Sirmatel et al., 2021; Zhong et al., 2017; Zhou and Gayah, 2021), the integration or comparison between the method proposed in this work and this literature in the future, in the context of traffic signal control resiliency, will also be a promising direction to be explored.

Acknowledgment

This research is supported by the National Science Foundation under Grant Number 1638301. Any opinions, findings, and conclusions or recommendations expressed in this manuscript are those of the authors and do not necessarily reflect the views of the National Science Foundation. The authors also want to thank Ali Shamansouri for running VISSIM simulations and helping collect system performance data.

References

Abiodun, O.I., Jantan, A., Omolara, A.E., Dada, K.V., Mohamed, N.A., Arshad, H., 2018. State-of-the-art in artificial neural network applications: A survey. *Heliyon* 4(11), e00938.

Bottou, L.J.O.-l.l.i.n.n., 1998. Online learning and stochastic approximations. 17(9), 142.

Brendel, W., Todorovic, S., 2011. Learning spatiotemporal graphs of human activities, *2011 International Conference on Computer Vision*. IEEE, pp. 778-785.

Cerrudo, C., 2015. An emerging US (and world) threat: Cities wide open to cyber attacks. *Securing Smart Cities* 17, 137-151.

Cui, Z.Y., Ke, R.M., Pu, Z.Y., Ma, X.L., Wang, Y.H., 2020. Learning traffic as a graph: A gated graph wavelet recurrent neural network for network-scale traffic prediction. *Transportation Research Part C-Emerging Technologies* 115, 15.

DHS, 2015. Transportation Systems Sector-Specific Plan-2015.

Dupond, S., 2019. A thorough review on the current advance of neural network structures. *Annual Reviews in Control* 14, 200-230.

Emtenan, A.T., Day, C.M., 2020. Impact of detector configuration on performance measurement and signal operations. *Transportation research record* 2674(4), 300-313.

Ernst, J.M., Michaels, A.J., 2017. Framework for Evaluating the Severity of Cybervulnerability of a Traffic Cabinet. *Transportation Research Record*(2619), 55-63.

FHWA, 2013. Highway Functional Classification Concepts, Criteria and Procedures. US Department of Transportation Washington, DC.

Gallagher, 2018. Driving toward security: Managing cyber liability risk in the transportation industry, https://www.ajg.com/media/1702480/transportationcampaign_whitepaper_cyber_hr.pdf.

Ganin, A.A., Mersky, A.C., Jin, A.S., Kitsak, M., Keisler, J.M., Linkov, I., 2019. Resilience in Intelligent Transportation Systems (ITS). *Transportation Research Part C* 100, 318-329.

Geroliminis, N., Daganzo, C.F., 2008. Existence of urban-scale macroscopic fundamental diagrams: Some experimental findings. *Transportation Research Part B: Methodological* 42(9), 759-770.

Ghena, B., Beyer, W., Hillaker, A., Pevarnek, J., Halderman, J.A., 2014. Green Lights Forever: Analyzing the Security of Traffic Infrastructure. *WOOT* 14, 7-7.

Graves, A., Liwicki, M., Fernández, S., Bertolami, R., Bunke, H., Schmidhuber, J., 2009. A Novel Connectionist System for Unconstrained Handwriting Recognition. *IEEE Transactions on Pattern Analysis and Machine Intelligence* 31(5), 855-868.

Guo, H., Zheng, C., Iu, H.H.-C., Fernando, T., 2017. A critical review of cascading failure analysis and modeling of power system. *Renewable and Sustainable Energy Reviews* 80, 9-22.

Guo, J., Huang, W., Williams, B.M., 2014. Adaptive Kalman filter approach for stochastic short-term traffic flow rate prediction and uncertainty quantification. *Transportation Research Part C: Emerging Technologies* 43, 50-64.

Halsey, A., 2009. Traffic Signals Disrupted, Creating Chaos in Montgomery. *Washington Post, November* 5.

Ho, Y.-C., Zhao, Q.-C., Jia, Q.-S., 2008. *Ordinal optimization: Soft optimization for hard problems*. Springer Science & Business Media.

Holling, C.S., 1973. Resilience and Stability of Ecological Systems. *Annual Review of Ecology and Systematics* 4(1), 1-23.

869 Jain, A., Zamir, A.R., Savarese, S., Saxena, A., 2016. Structural-rnn: Deep learning on spatio-
870 temporal graphs, *Proceedings of the ieee conference on computer vision and pattern*
871 *recognition*, pp. 5308-5317.
872 Juan, A.A., Faulin, J., Grasman, S.E., Rabe, M., Figueira, G., 2015. A review of simheuristics:
873 Extending metaheuristics to deal with stochastic combinatorial optimization problems.
874 *Operations Research Perspectives* 2, 62-72.
875 Kim, Y., Wang, P., Mihaylova, L., 2019. Scalable Learning With a Structural Recurrent Neural
876 Network for Short-Term Traffic Prediction. *IEEE Sensors Journal* 19(23), 11359-11366.
877 Kim, Y., Wang, P., Zhu, Y., Mihaylova, L., 2018. A capsule network for traffic speed prediction
878 in complex road networks, *2018 Sensor Data Fusion: Trends, Solutions, Applications*. IEEE,
879 pp. 1-6.
880 Koppula, H., Saxena, A., 2013. Learning spatio-temporal structure from rgb-d videos for human
881 activity detection and anticipation, *International conference on machine learning*, pp. 792-
882 800.
883 Kschischang, F.R., Frey, B.J., Loeliger, H., 2001. Factor graphs and the sum-product algorithm.
884 *IEEE Transactions on Information Theory* 47(2), 498-519.
885 Lev, G., Sadeh, G., Klein, B., Wolf, L., 2016. RNN fisher vectors for action recognition and
886 image annotation, *European Conference on Computer Vision*. Springer, pp. 833-850.
887 Li, X., Wu, X., 2015. Constructing long short-term memory based deep recurrent neural
888 networks for large vocabulary speech recognition, *2015 IEEE International Conference on*
889 *Acoustics, Speech and Signal Processing (ICASSP)*. IEEE, pp. 4520-4524.
890 Lv, Y., Duan, Y., Kang, W., Li, Z., Wang, F.-Y., 2014. Traffic flow prediction with big data: a
891 deep learning approach. *IEEE Trans. Intell. Transp. Syst.* 16(2), 865-873.
892 Ma, X., Dai, Z., He, Z., Ma, J., Wang, Y., Wang, Y., 2017. Learning traffic as images: a deep
893 convolutional neural network for large-scale transportation network speed prediction.
894 *Sensors* 17(4), 818.
895 Ma, X., Yu, H., Wang, Y., Wang, Y., 2015. Large-scale transportation network congestion
896 evolution prediction using deep learning theory. *PloS one* 10(3), e0119044.
897 Mattsson, L.-G., Jenelius, E., 2015. Vulnerability and resilience of transport systems – A
898 discussion of recent research. *Transportation Research Part A: Policy and Practice* 81, 16-
899 34.
900 Mei, Z., Tan, Z., Zhang, W., Wang, D., 2019. Simulation analysis of traffic signal control and
901 transit signal priority strategies under Arterial Coordination Conditions. *Simulation* 95(1),
902 51-64.
903 Mercader, P., Haddad, J., 2021. Resilient multivariable perimeter control of urban road networks
904 under cyberattacks. *Control Engineering Practice* 109, 104718.
905 Mohebbi, S., Zhang, Q., Wells, E.C., Zhao, T., Nguyen, H., Li, M., Abdel-Mottaleb, N., Uddin,
906 S., Lu, Q., Wakhungu, M., 2020. Cyber-Physical-Social Interdependencies and
907 Organizational Resilience: A Review of Water, Transportation, and Cyber Infrastructure
908 Systems and Processes. *Sustainable Cities and Society*, 102327.
909 NGA, 1979. Comprehensive emergency management: A governor's guide, in: National
910 Governors' Association, C.f.P.R.D.o.D., Defense Civil Preparedness Agency (Ed.).
911 Oricchio, V., Hunter, M., Jared, D., 2008. Microscopic Simulation Model of Traffic Operations
912 at Intersections in Malfunction Flash Mode. *Transportation Research Record* 2080, 67-74.
913 Osorio, C., Bierlaire, M., 2013. A simulation-based optimization framework for urban
914 transportation problems. *Operations Research* 61(6), 1333-1345.

Osorio, C., Chong, L., 2015. A computationally efficient simulation-based optimization algorithm for large-scale urban transportation problems. *Transportation Science*(3), 623.
Osorio, C., Wang, C., 2017. On the analytical approximation of joint aggregate queue-length distributions for traffic networks: A stationary finite capacity Markovian network approach. *Transportation Research Part B: Methodological* 95, 305-339.
Reilly, J., Martin, S., Payer, M., Bayen, A.M., 2016. Creating complex congestion patterns via multi-objective optimal freeway traffic control with application to cyber-security. *Transportation Research Part B: Methodological* 91, 366-382.
Ren, Y., Hou, Z., Sirmatel, I.I., Geroliminis, N., 2020. Data driven model free adaptive iterative learning perimeter control for large-scale urban road networks. *Transportation Research Part C: Emerging Technologies* 115, 102618.
Sadler, J., Goodall, J., Morsy, M., Spencer, K., 2018. Modeling urban coastal flood severity from crowd-sourced flood reports using Poisson regression and Random Forest. *Journal of hydrology* 559, 43-55.
Sak, H., Senior, A.W., Beaufays, F., 2014. Long short-term memory recurrent neural network architectures for large scale acoustic modeling.
Shekhar, S., Williams, B.M.J.T.R.R., 2007. Adaptive seasonal time series models for forecasting short-term traffic flow. 2024(1), 116-125.
Sirmatel, I.I., Tsitsokas, D., Kouvelas, A., Geroliminis, N., 2021. Modeling, estimation, and control in large-scale urban road networks with remaining travel distance dynamics. *Transportation Research Part C: Emerging Technologies* 128, 103157.
Sra, S., Nowozin, S., Wright, S.J., 2012. *Optimization for machine learning*. Mit Press.
Tealab, A., 2018. Time series forecasting using artificial neural networks methodologies: A systematic review. *Future Computing and Informatics Journal* 3(2), 334-340.
Teney, D., Liu, L., van Den Hengel, A., 2017. Graph-structured representations for visual question answering, *Proceedings of the IEEE conference on computer vision and pattern recognition*, pp. 1-9.
Vemula, A., Muelling, K., Oh, J., 2018. Social attention: Modeling attention in human crowds, *2018 IEEE international Conference on Robotics and Automation (ICRA)*. IEEE, pp. 1-7.
Walker, B., Carpenter, S., Anderies, J., Abel, N., Cumming, G., Janssen, M., Lebel, L., Norberg, J., Peterson, G.D., Pritchard, R., 2002. Resilience Management in Social-ecological Systems a Working Hypothesis for a Participatory Approach. *Conservation Ecology* 6(1).
Wang, X., Shahidehpour, M., Jiang, C., Li, Z., 2018. Resilience enhancement strategies for power distribution network coupled with urban transportation system. *IEEE Transactions on Smart Grid*.
Waze-Maps, 2018. Idaho's Statewide Systems Map, Functional Classification.
Wright, C., Roberg, P., 1998. The conceptual structure of traffic jams. *Transport Policy* 5(1), 23-35.
Wu, Y., Tan, H., Qin, L., Ran, B., Jiang, Z., 2018. A hybrid deep learning based traffic flow prediction method and its understanding. *Transportation Research Part C: Emerging Technologies* 90, 166-180.
Xu, B., Shen, H., Cao, Q., Qiu, Y., Cheng, X., 2019. Graph wavelet neural network. *arXiv preprint arXiv:.07785*.
Yan, S., Xiong, Y., Lin, D., 2018. Spatial temporal graph convolutional networks for skeleton-based action recognition, *Thirty-second AAAI conference on artificial intelligence*.

Yin, W., Kann, K., Yu, M., Schütze, H., 2017. Comparative study of cnn and rnn for natural language processing. *arXiv preprint arXiv:.01923*.
Zhang, J., Zheng, Y., Qi, D., 2017. Deep spatio-temporal residual networks for citywide crowd flows prediction, *Thirty-First AAAI Conference on Artificial Intelligence*.
Zhong, R.X., Chen, C., Huang, Y.P., Sumalee, A., Lam, W.H.K., Xu, D.B., 2017. Robust Perimeter Control for Two Urban Regions with Macroscopic Fundamental Diagrams: A Control-Lyapunov Function Approach. *Transportation Research Procedia* 23, 922-941.
Zhou, D., Gayah, V.V., 2021. Model-free perimeter metering control for two-region urban networks using deep reinforcement learning. *Transportation Research Part C: Emerging Technologies* 124, 102949.
Zou, Q.L., Chen, S.R., 2019. Enhancing resilience of interdependent traffic-electric power system. *Reliability Engineering & System Safety* 191, 18.

Appendix

Based on the total delay curves of the case study presented in Section 4, it is observed that the combinations of the same number of failed signals could lead to significantly different network performance during restoration. This appendix further illustrates this observation from a Macroscopic Fundamental Diagram (MFD) point of view. Geroliminis and Daganzo (Geroliminis and Daganzo, 2008) proved the existence of MFDs in urban road networks, revealing the relationship between outflow and accumulation in a network. For a given failure scenario S_i =[I_1, I_2, I_3, …, I_k] with k signals failed (I_j is the index of the jth failed signal; The scenarios are studied with all k signals failed simultaneously), and MFD is constructed by running simulations with various demand levels (multiplying a coefficient [120%, 115%, 110%, … 70%] to the original input flows into the studied network) and obtaining the observations of outflow and accumulation in the network every 10 mins after 50 minutes of warm-up.

As shown in Fig. A.1, the horizontal axis is the accumulation of vehicles, i.e., the total number of vehicles in the system at the middle of one time interval, and the vertical axis is the weighted flow, i.e., the weighted average flow by the length of the lane that follows the calculation method in Geroliminis and Daganzo's work (Geroliminis and Daganzo, 2008). Specifically, i is the index for a road lane and l_i is its length; q_i is the flow measured by a detector on this lane in a particular time interval. The weighted average flow is calculated as

$$q^w = \left(\sum_i q_i l_i\right) / \sum_i l_i$$

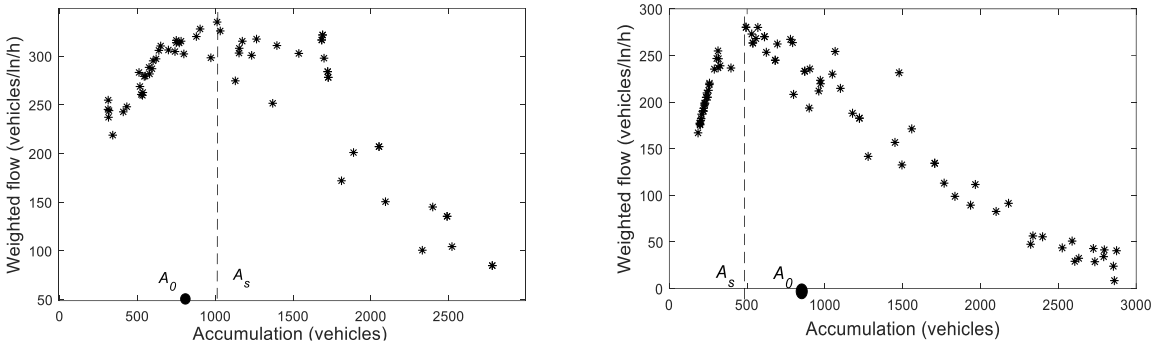

Fig. A.1. MFDs of the case study network with 6 signals failed.
(a) Scenario I [2,6,7,13,14,16]; (b) Scenario II [2,7,8,13,14,24]

The A_s is the "sweet spot" of MFD, i.e., the accumulation (vehicles) in the system when the outflow is the maximum. A_0, the accumulation (vehicles) at the end of 50 minutes of warm-up for a normal network (without signal failure), is also shown in Fig. A.1. Therefore, A_s is the "sweet spot" of the MFD for the network with selected signals failed and indicates the network level capacity of the deteriorated network. A_0 is the accumulation of vehicles at the end of normal status, i.e., just before signal failure occurring, and indicates the number of vehicles that need to be served by the deteriorated network. Two types of failure scenarios are defined according to the comparison between A_s and A_0 to facilitate further discussion, i.e., Type I scenario with $A_0 < A_s$ and Type II scenario with $A_0 > A_s$.

Fig. A.1 shows the MFD of Scenarios I and II, indicating that Scenario I is a typical Type I scenario, with $A_s > A_0$, and Scenario II is a typical Type II scenario, with $A_s < A_0$. The basic idea is that the comparison between A_s and A_0 can help determine whether the deteriorated network can serve the accumulation of vehicles efficiently, recalling the three representative regions on MFDs—"free flow region," "maximum flow region," and "congested flow region" (Geroliminis and Daganzo, 2008). Cross-referencing to Fig. 6, Scenario I, as a Type I scenario, can better serve the accumulation of vehicles, compared to the Scenario II, as a Type II scenario. Furthermore, the restoration sequence optimization is more critical for Type II scenario as less portion of the feasible sequences, compared to Type I scenario, could mitigate the congestion caused by the signal failure, as shown in Fig. 6. Therefore, the MFD perspective can help to understand the difference of the impacts on system performance between the two types of scenarios, as exemplified in Fig. 6.